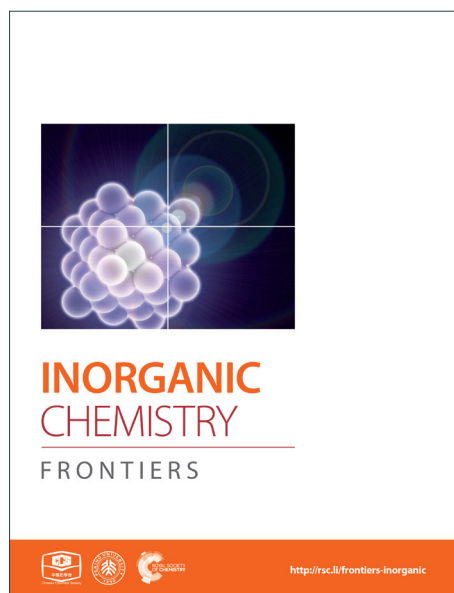
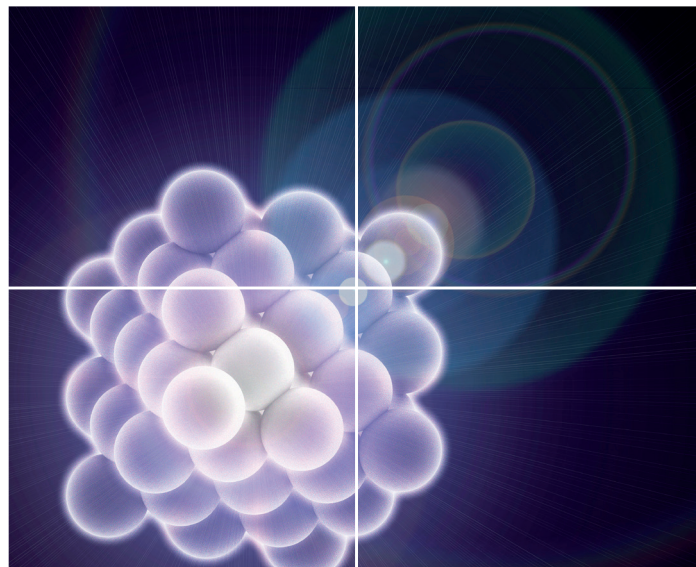


INORGANIC CHEMISTRY

FRONTIERS

Accepted Manuscript



This is an *Accepted Manuscript*, which has been through the Royal Society of Chemistry peer review process and has been accepted for publication.

Accepted Manuscripts are published online shortly after acceptance, before technical editing, formatting and proof reading. Using this free service, authors can make their results available to the community, in citable form, before we publish the edited article. We will replace this *Accepted Manuscript* with the edited and formatted *Advance Article* as soon as it is available.

You can find more information about *Accepted Manuscripts* in the [Information for Authors](#).

Please note that technical editing may introduce minor changes to the text and/or graphics, which may alter content. The journal's standard [Terms & Conditions](#) and the [Ethical guidelines](#) still apply. In no event shall the Royal Society of Chemistry be held responsible for any errors or omissions in this *Accepted Manuscript* or any consequences arising from the use of any information it contains.

Diazopyridine-Ni(II) Complexes Exhibiting Intra-Chain Ferromagnetic Interaction After Irradiation: Formation of Magnetic Gel

Koya Mori,¹ Rumi Eguchi,¹ Satoru Karasawa,^{1,2,*} and Noboru Koga^{1,*}

¹. Graduate School of Pharmaceutical Sciences, Kyushu University, 3-1-1 Maidashi, Higashi-ku, Fukuoka, 812-8582 Japan

². PRESTO, Japan Science and Technology Agency, Kawaguchi, 332-0012 Japan

*Corresponding authors

Tel ; +81-92-642-6593. Fax +81-92-642-6545

E-mail: karasawa@fc.phar.kyushu-u.ac.jp and koga@fc.phar.kyushu-u.ac.jp

Abstract.

Diazopyridine-nickel complexes, **1** and **2**, were obtained by mixing di(4-pyridyl)diazomethane, **D1py**₂, with Ni(**R-hfpip**)₂; hfpip = 4-(4-R-phenylimino)-1,1,1,5,5,5-hexafluoro-2-pentanone and R = *n*-hexyl (**1**) and *n*-octyl (**2**), in a 1:1 ratio. The discrete reference complex [Ni(*n*-hexyl-hfpip)(**4NOpy**)₂] (**3**) was also prepared. In the tube inversion test and the rheological measurements, the sample (20 mM) of **1** and **2** dissolved in EtOH-20 % CH₂Cl₂ solution showed gelation behavior at -4 °C. In scanning transmission microscopy (SEM) image of the xerogel sample, fibers with widths of 500 - 700 nm were observed. Vis-NIR spectrum of the gel sample for **1** showed the typical broad absorption at ~ 995 nm due to the octahedral Ni(II) complex, suggesting that the pyridine ligands in **D1py**₂ coordinated to the Ni(II) ion to form the chain structure. Complex **3** showed ferromagnetic interaction with $J/k_B = 26.7$ K between the aminoxyl and the Ni(II) through the pyridine ring. Similarly, the thermal profile of χ_{mol} values after irradiation of the gel sample of **1** showed a ferromagnetic interaction between the generated triplet carbenes and the Ni(II) ions and

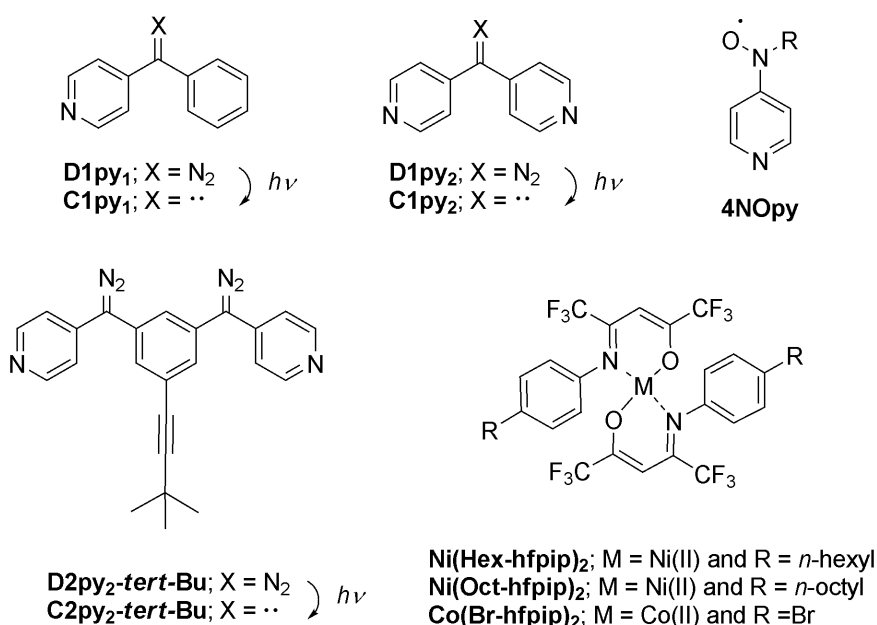
provided a magnetic chain structure. The magnetic correlation length was estimated to be 4 - 5 units from the maximum value of $\chi_{\text{mol}}T$ ($12.7 \text{ cm}^3 \text{ K mol}^{-1}$ at 7 K).

1. Introduction.

Quantum magnets having large magnetic anisotropy (D and E) such as single-molecule magnets (SMMs)^[1], single-chain magnets (SCMs)^[2], and single-ion magnets (SIMs)^[3] have been extensively studied in the field of molecule-based magnets. Their application to molecular memory, magnetic devices, and quantum computers is anticipated.^[4] We have been studying a heterospin system^[5] consisting of organic spins and 3d transition metal ions in the field of molecule-based magnets^[6]. In this heterospin system, the organic spins of aminoxyl, **4NOpy**,^[7] and triplet carbene generated by photolysis of diazo groups, **D1py**,^[8] **D1py**₂,^[9] and **D2py**₂,^[10] were used. By using the latter spin source, the mono- and dinuclear octahedral cobalt complexes, were reported to show SMMs behaviors after irradiation in solid and frozen solution conditions.^[11] The obtained SMMs had large activation barriers and hysteresis loops of magnetization with large coercive forces. To develop the field of molecule-based magnets, the construction of new functional materials having a magnetic properties is interesting and significant. This time, our heterospin systems were combined with gel, being soft materials and the construction of the *magnetic gel* exhibiting intense magnetic interaction was studied. Gels have been widely studied and used in various fields such as tissue engineering,^[12] cell batteries,^[13] photo devices,^[14] and environmental materials.^[15] Recently, not only general gels made of polymers and organic molecules^[16] but also metallo gels^[17] containing metal ions and/or metal complexes have been developed and examined. The crystals and powders naturally exhibited the magnetic properties of solid state. In contrast, the gel potentially have both properties of the solid state and solution state, which are shown as the values of G' and G'' in rheological measurement.^{[16][17]} Therefore, the magnetic properties of gel should exhibit the both properties of the solid and

solution state. Furthermore, the gel and the crystals (powders) favor the structures of kinetically stable and thermodynamically stable, respectively. Accordingly, we can investigate the magnetic properties of kinetically stable structure of the materials by the gel samples.

We have also studied the gelation behaviors of aromatic compounds having the urea unit, alkyl chain, and oligoethyleneglycol units.^[18] Generally, the structure of gels obtained from polymers^[19] and supra-molecules^[20] is a 3-D network consisting of 1-D fibers. Accordingly, we applied our heterospin chain as the main framework of gel structure and used a combination of **D1py**₂ and **M(R-hfpip)**₂; R-hfpip = 4-(4-R-phenylimino)-1,1,1,5,5,5-hexafluoropentanone. The combination of **D1py**₂ and **Co(Br-hfpip)**₂ was reported to form chain complexes of **[Co(Br-hfpip)₂D1py₂]_n** showing SCMs like magnetic behaviors.^[21] For gel formation, first, the alkyl-chain substituents, *n*-hexyl and *n*-octyl, were attached to the hfpip ligand. The complexes obtained from **D1py**₂ and **Ni(R-hfpip)**₂; R = *n*-hexyl and *n*-octyl, were expected to form a metallogel and a magnetic gel. Herein, we describe the formation of magnetic gel, its morphology, and its magnetic behavior before and after irradiation.



Scheme 1. Formula of pyridine derivatives carrying diazo and aminoxy, and $M(R\text{-hfpip})_2$ complexes.

2. Experimentals.

2-1. Materials: Unless otherwise stated, the preparative reactions were carried out under a high purity dry nitrogen atmosphere. Diethylether, tetrahydrofuran (THF), and 2-methyltetrahydrofuran (MTHF), were distilled from sodium benzophenone ketyl. Dichloromethane and acetonitrile were distilled by CaH_2 . **D1py₂** and **4NOpy** were prepared in a manner similar to the procedure reported previously.^[5a]

4-(*n*-hexyl-phenylimino)-1,1,1,5,5,5-hexafluoro-2-pentanone, Hex-hfpip: To a solution (18 ml) of *p*-hexylaniline (3 ml, 15.6 mmol) in CHCl_3 was added montmorillonite K10 (3.6 g) and 1,1,1,5,5,5-hexafluoropentane-2,4-dione, hfac, (2.2 ml, 15.6 mmol) and the mixture was stirred at 70 °C for 15 hr. The solution was cooled to r.t., the inorganic catalysis was filtrated and the solution was evaporated by reduced pressure to afford the reddish black oils. The crude residue was chromatographed on silica gel using *n*-hexane : AcOEt (40 :1) as elute to separately afford the yellow oil in 84 % yield (4.8 g, 13.1 mmol). ¹HNMR (500 MHz, CDCl_3); δ 11.9 (*s*, 1H), 7.22 (*d*, $J = 8.5$ Hz, 2H), 7.15 (*d*, $J = 8.5$ Hz, 2H), 6.01 (*s*, 1H), 2.63 (*t*, $J = 7.8$ Hz, 2H), 1.62 (*quin*, $J = 7.8$ Hz, 2H), 1.36 – 1.27 (*m*, 6H), 0.88 (*t*, $J = 6.5$ Hz, 3H). FAB-MS; 367.1[M]⁺. Anal. Calcd. for $\text{C}_{17}\text{H}_{19}\text{F}_6\text{NO}$, C 55.59, H 5.21, N 3.81, found C 55.29, H 4.99, N 3.91.

4-(*n*-octyl-phenylimino)-1,1,1,5,5,5-hexafluoro-2-pentanone, Oct-hfpip: This was prepared in a manner similar procedure to **Hex-hfpip** by replacing *p*-octylamine with *p*-hexylaniline. The crude residue was chromatographed on silica gel using *n*-hexane : AcOEt (40 :1) as elute to separately afford the yellow oil in 76 % yield. ¹HNMR (500 MHz, CDCl_3); δ 11.9 (*s*, 1H), 7.22 (*d*, $J = 8.5$ Hz, 2H), 7.15 (*d*, $J = 8.5$ Hz, 2H), 6.01 (*s*, 1H), 2.63 (*t*, $J = 7.8$ Hz, 2H), 1.62 (*quin*, $J = 7.8$ Hz, 2H), 1.36

– 1.27 (*m*, 10H), 0.88 (*t*, $J = 6.5$ Hz, 3H). FAB-MS; 395.0[M]⁺. Anal. Calcd. for C₁₉H₂₃F₆NO, C 57.72, H 5.86, N 3.54, found C 57.79, H 5.89, N 3.61.

1: To a solution (1 ml) of **Hex-hfpip** (800 mg, 2.2 mmol) in MeOH was added aqueous solution (3 ml) of NaOH (90 mg, 2.3 mmol) and the solution was stirred vigorously for 5 min. To the solution was added aqueous solution (2 ml) of NiCl₂ 6H₂O and subsequently stirred vigorously for 30 min. After filtration, the residue was dissolved by CH₂Cl₂ and dried over MgSO₄. The solvent was evaporated to afford **Ni(Hex-hfpip)₂** (869 mg, 1.1 mmol) as dark green oil. The nickel complex was used for the next step without further purification. The solution (1 ml) of **D1py₂** (74 mg, 0.38 mmol) in CH₂Cl₂ was mixed with the solution (1 ml) of **Ni(Hex-hfpip)₂** (300 mg, 0.38 mmol) in CH₂Cl₂ and then MeOH (8 ml) was added. The resulting yellow precipitate was collected by a suction filtration and was washed with MeOH. **1** was obtained as yellow powder in 34 % yield (125 mg, 0.13 mmol). IR (KBr); $\nu(\text{N}_2)$; 2063 cm⁻¹. M.P.(decomp.); 185°C. Anal. Calcd. for C₄₅H₄₄F₁₂N₆NiO₂•0.5CH₂Cl₂, C 53.06, H 4.40, N 8.16, found C 53.13, H 4.44, N 8.27.

2: To a solution (1 ml) of **Oct-hfpip** (869 mg, 2.2 mmol) in MeOH was added aqueous solution (3 ml) NaOH (90 mg, 2.3 mmol). The solution was stirred vigorously for 5 min, aqueous solution (2 ml) of NiCl₂ 6H₂O (259 mg, 1.1 mmol) was added, and then subsequently stirred vigorously for 30 min. After filtration, the residue was dissolved in CH₂Cl₂ and dried over MgSO₄. The solvent was evaporated to afford **Ni(Oct-hfpip)₂** (844 mg) as dark green oil. The obtained nickel complex was used for the next step without further purification. The solution (1 ml) of **D1py₂** (69 mg, 0.36 mmol) in CH₂Cl₂ was mixed with the solution (1 ml) of **Ni(Oct-hfpip)₂** (300 mg, 0.36 mmol) in CH₂Cl₂ and then MeOH (8 ml) was added. The resulting yellow precipitates was collected by a suction filtration and was washed with MeOH. **2** was obtained as yellow powders in 50 % yield (198 mg, 0.18 mmol). IR (KBr); $\nu(\text{N}_2)$; 2063 cm⁻¹. M.P. (decomp.); 143 °C. Anal. Calcd. for C₄₉H₅₂F₁₂N₆NiO₂, C 56.39, H 5.02, N 8.05, found C 56.29, H 4.99, N 7.91.

3: To a solution (10 ml) of hydroxylamine of 4NOHpy (70 mg, 0.42 mmol) in CH₂Cl₂ was added Ag₂O (0.7 g, 3 mmol) and the solution was stirred for 10 min. After removal of Ag₂O by filtration, the filtrate containing **4NOpy** was added to the solution (10 ml) of Ni(**Hex-hfpip**)₂ (170 mg, 0.21 mmol) in CH₃CN. The solution was condensed by reduced pressure and left at -30°C. **3** was obtained as red blocks in 10 % yield (27.0 mg, 0.022 mmol). M.P.; 112 - 116°C. Anal. Calcd. for C₅₂H₆₂F₁₂N₆NiO₄, C 55.68, H 5.57, N 7.49, found C 55.73, H 5.65, N 7.47.

2-2. General Methods: Infrared spectra were recorded on a JASCO 420 FT-IR spectrometer. ¹H NMR spectra were measured on a Bruker Biospin AVANCE III 500 Fourier transform spectrometer using CDCl₃ as solvent and referenced to TMS. FAB mass spectra (FAB MS) by using 4-nitrobenzylalcohol (NBA) as a matrix were recorded on a JEOL JMS-SX102 spectrometer. UV-Vis infrared spectra were recorded on a JASCO V570 spectrometer. Scanning electron microscopy (SEM) was carried out on a Shimadzu Superscan SSX-550. Melting points and phase transition temperatures were determined by DSC. Powder X-ray diffraction (PXRD) measurements were performed by Bruker SAXS NANOSTAR in 2θ range of 2 - 10° at 23 °C. Rheological measurements were performed by an Anton Parr MCR 301 rheometer. Elemental analyses were performed at the Analytical Center of the Faculty of Science in Kyushu University.

2-3. Single crystal X-ray diffraction (SXRD): Suitable single crystal was glued onto a glass fiber using epoxy resin. X-ray diffraction data were collected on a Rigaku RAXIS-RAPID diffractometer with graphite monochromated CuK_α radiation (λ = 1.54187 Å) for **3**. Reflections were collected at 123 ± 1 K. The molecular structures were solved by direct methods (SHELXL 97).^[22] The refinements were converged using the full-matrix least squares method from the Crystal Structure software package^[23] to give P2₁/c (no. 14) for **3**. All non-hydrogen atoms were refined anisotropically and hydrogen atoms were refined isotropically. Crystallographic data collection and structural refinement information for **3** are listed in Table S1. Crystallographic data for the structure

reported in this paper have been deposited with the Cambridge Crystallographic Data Center as supplementary publication no. CCDC 1406724.

2-4. SQUID measurements: Direct current (dc) magnetic susceptibility data were obtained with a Quantum Design MPMS2 SQUID magneto/susceptometer, and corrected for the magnetization of the sample holder, capsule, and cellophane tape, and/or diamagnetic contributions to the samples, which were estimated from Pascal constants. ^[6]

A hand-made irradiation system^[5a] was used for photolysis of diazo chromophore inside the SQUID apparatus. For the effective photolysis of diazo-nickel complex with its irradiation system, less than 1 mg of powder was used and the 10 – 20 mM concentration for the gel and frozen solution were used. In such small amounts of spins, the temperatures at 10 and 50 K before and after irradiation, respectively, were the highest temperature possible to measure the paramagnetic susceptibility. To avoid raising the temperature and decomposing the sample by local heating, the cooling value maintained to open in SQUID apparatus during irradiation.

3. Results and discussion.

3-1. Preparation: **D1py₂** and **4NOpy** were prepared by the procedure reported previously. R-Hfpip; 4-(4-R-phenylimino)-1,1,1,5,5,5-hexafluoropentanone (R = *n*-hexyl and *n*-octyl) were prepared by the condensation reaction of 1,1,1,5,5,5-hexafluoropentane-2,4-dione, hfac, with the corresponding para substituted aniline in the presence of the dehydration catalyst of montmorillonite K10. **Ni(R-hfpip)₂** were prepared by the reaction of R-hfpip and NiCl₂·6H₂O in basic condition. **D1py₂** was mixed with **Ni(R-hfpip)₂** to afford **1** (R = *n*-hexyl) and **2** (R = *n*-octyl) as yellowish powders. To understand the magnetic property between the nickel ion and the organic spin through pyridine rings, the stable radical, **4NOpy** was used in place of the **D1py₂** and the discrete nickel complex, **Ni(Hex-hfpip)₂(4NOpy)₂**, was prepared as a reference complex, **3**. The reference complex

3 was prepared in a manner similar to the procedure for **1** and was obtained as a single crystal of red block.

3-2. Crystal Structure; The crystal structure of single crystals for **3** was analyzed by X-ray crystallography. The measurement was performed by Cu radiation at 123 K and the diffraction data were analyzed by SHELXL 97 software.^[22] Discrete heterospin nickel complex **3** was crystallized in the space group of $P2_1/c$ (no 14) with $Z = 4$ ($Z' = 1$). Crystallographic data collection and structural refinement information for **3** is shown in Table S1.

In **3**, the pyridine rings of two **4NOpy** coordinated to the Ni(II) ion in *cis* configuration. The molecular structure was a compressed octahedron, in which the bond distances between the Ni(II) ion and the O atoms of hfpip were short. The molecular structure and the crystal packing with short contacts of **3** are shown in Figure 1, and the full structure of **3** is shown in Figure S1.

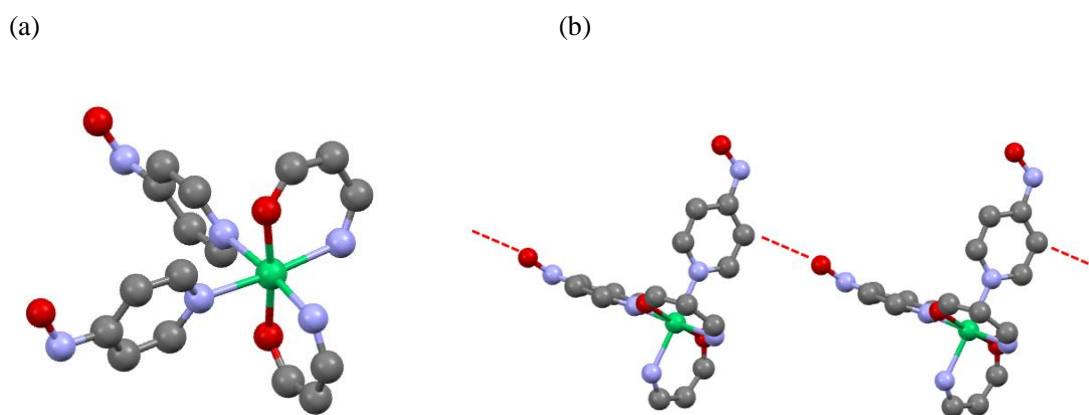


Figure 1. Molecular structure (a) and crystal packing (b) of **3** with a ball and stick model; color code: Ni, (green), N (blue), O (red), and C (gray). Red dotted lines in (b) indicate short distance of 3.194(3) Å between NO and C(β) in Py ring. Phenyl, *tert*-Bu, CF₃, and hexyl group and H atoms are omitted for a sake of clarity.

The bond distances around the Ni(II) ion were $r_{\text{Ni-Nimi}} = 2.127(3)$ and $2.123(3)$ Å with the N atoms of hfpip, $r_{\text{Ni-Npy}} = 2.154(3)$ and $2.160(3)$ Å with the N atoms of pyridine rings, and $r_{\text{Ni-o}} = 1.992(3)$ and $2.003(3)$ Å with the O atoms of hfpip,. The dihedral angles between the XY plane defined by the four N atoms coordinating to the Ni(II) ion and two pyridine rings were $71.57(0.06)^\circ$ and $77.94(0.06)^\circ$. The dihedral angles between the pyridine ring and the NO plane were $2.74(0.16)$ and $22.42(0.19)^\circ$. Those bond lengths and the dihedral angles suggested that the magnetic interaction might take place effectively between Ni(II) ion and the aminoxyl through pyridine rings.^[5a] Selected bond lengths and dihedral angles of **3** are listed in Table 1.

Table 1. Selected bond lengths and dihedral angles of **3** with estimated standard deviation in parentheses.

Bond lengths of coordination site in Ni ion / Å	
$r_{\text{Ni - Npy}}$	2.154(3) and 2.160(3)
$r_{\text{Ni - Nimi}}$	2.123(3) and 2.127(3)
$r_{\text{Ni - O}}$	1.992(3) and 2.003(3)
Dihedral angles between XY plane and pyridine rings / °	
XY-py	71.57(0.06) and 77.94(0.06)
Dihedral angles between pyridine and NO / °	
py-NO	2.74 (0.16) and 22.42 (0.19)

In crystal packing, intermolecular short contacts (red dotted line in Figure 1) were observed and the distance, $r_{\text{O-C}}$, between the O atom of aminoxyl center and the C(β) atom at the position of β of the pyridine ring was $3.194(3)$ Å. This short contact is often observed in heterospin systems using

aminoxyl as organic spin.^[5a] The observed short contacts might cause the intermolecular magnetic interaction through the space of the cryogenic temperatures.

3-3. Gelation test and rheological measurements for 1 and 2: To confirm gel formation, the gel tests for **1** and **2** were carried out. The complexes were dissolved in 13 solvents and then 20 mM solution samples were prepared. Each sample was kept at -4 °C and the solutions after 24 h were visually confirmed (Table 2). For **1** having *n*-hexyl group, the solubility for alcohols (entry 1 - 3 in Table 2) and aliphatic hydrocarbon (entry 12 - 14) solvents was poor and the precipitates appeared immediately after dissolving in the solvents. In contrast, the solubility in halogenated (entry 8 and 9), ethereal (entry 6, 7 and 11), and aprotic polar (entry 4, 5 and 10) solvents was high and the solutions were maintained even at -4 °C. Therefore, the mixed solvents of CH₂Cl₂ and EtOH, which were good and medium/poor solvents, respectively, were used as the solvent for **1**. In EtOH solutions containing 20 – 40 % CH₂Cl₂ (20 - 40%CH₂Cl₂/EtOH, entry 15 - 17), increase in the solvent viscosity was observed. By the tube inversion test,^[24] the sample dissolved in 20% CH₂Cl₂/EtOH (entry 16) became a transparent gel at -4°C and the gel was maintained for more than 6 hr at r.t. (Figure 2). In contrast, 11 mM samples dissolved in 20% CH₂Cl₂/EtOH showed no gelation behavior. Furthermore, **2** having the *n*-octyl group showed similar solubility to **1** against 13 solvents and the gel accompanied with the powder was obtained under 20% CH₂Cl₂/EtOH (entry 16) condition. Photographs of the gel and sol sample for **1** are shown in Figure 2 and the tests for the gelation in various solvents are summarized in Table 2.



Figure 2. Photographs of “sol” (left) and “gel” (right) samples for **1** at rt: solutions (20 mM) dissolved in 20% CH₂Cl₂/EtOH at rt.

Table 2. Organic solvents tested for gelation with **1** and **2** (20 mM).

entry	solvents	1	2
1	MeOH	S(h) → P	S(h) → P
2	EtOH	S(h) → P	S(h) → P
3	BuOH	I	I
4	MeCN	I	I
5	Acetone	S	S
6	MTHF	S	S
7	1,4-dioxane	S	S
8	CH ₂ Cl ₂	S	S
9	CHCl ₃	S	S
10	AcOEt	S	S → P
11	Et ₂ O	S	S
12	<i>n</i> -Hexane	I	I
13	<i>c</i> -Hexane	S(h)	S(h) → P
14	toluene	S(h)	S(h) → P + WG
15	10%CH ₂ Cl ₂ /EtOH	S → P	S → P
16	20%CH ₂ Cl ₂ /EtOH	G	S → P + G
17	40%CH ₂ Cl ₂ /EtOH	WG	S

S, S(h), I, P, G, and WG denote solution, solution by heating, insoluble, precipitation, gel, and weak gel, respectively.

Rheological measurements of the obtained gel samples for **1** (entry 16 and 17) and **2** (entry 16) were carried out at 23 °C.^[25] The gel samples were prepared in a parallel-type plates with a diameter of 50 mm and set in a rheometer. The strain ($\gamma / \%$) dependence of the values of elastic modulus (G') and viscous modulus (G'') are shown in Figure 3 for **1** and S2 for **2**. In the measurements, the oscillating frequency of 1 Hz was used under sweeping strain, γ , from 0.01 to 1000 %. The G' and G'' indicate the ability which a deformed material changed its original geometry back and the tendency of a material to flow, respectively. Therefore those rheological parameters provide the gel properties for the hardness and the softness from the value of G' in low γ region, and the stability and the strength by mechanical stress from an inflection point of G' value by changing the mechanical strain. The typical gel samples exhibit that the G' value independent upon strain until broken the formation and furthermore the G' exceed the G'' by about one order magnitude.^[26]

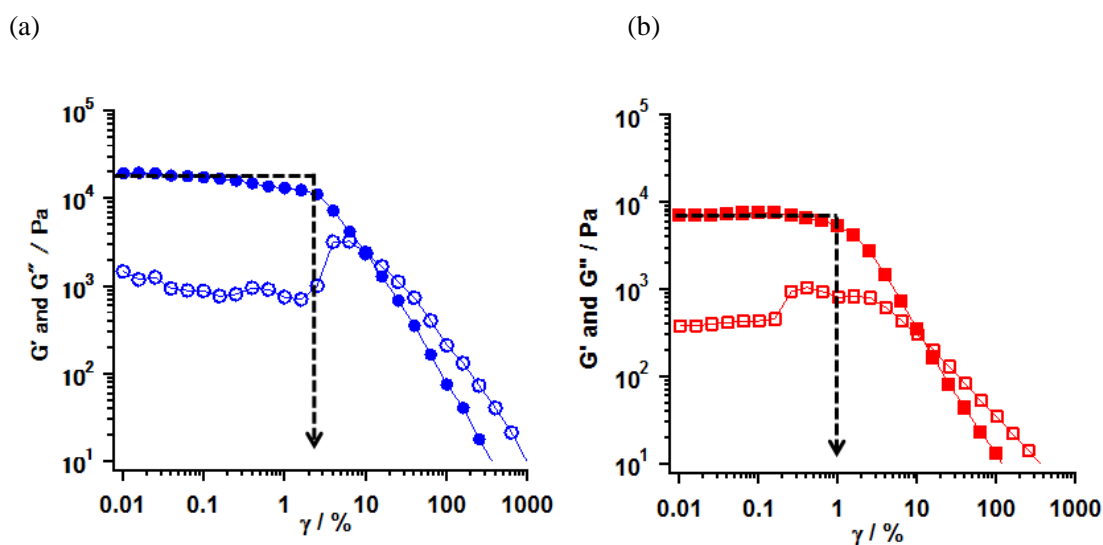


Figure 3. Strain dependence of G' (filled circles or squares) and G'' (empty circles and square) of the gel **1** obtained according to condition in entry 16 (a) and entry 17 (b). The dotted lines parallel to the horizontal axes and the dotted arrows indicate the plateau regions of G' values in low γ regions and inflection points of G' values upon increasing the strain.

In the gel sample of **1** (entry 16), the G' values in low γ regions were plateau around $1.2 - 1.8 \times 10$ kPa. In this region, the G' values were one order magnitude larger than one of the G'' , indicating that the gel behaves as elastic solid. As increasing the strain, an inflection point of the G' value was observed at $\gamma = 2.5$ % and the magnitude of G'' values exceeded G' values above 20 % strain ($G' < G''$), indicating that the gel (entry 16) behave as viscous solution and the transformation from gel to sol took place at the point. In contrast, the weak gel sample of **1** (entry 17), the G' values showed the plateau around $6.6 - 7.1$ kPa in low γ region and an inflection point was observed at 0.63 % strain. Furthermore, the transformation took place at 10 % strain. When compared the properties of those gels, the gel (entry 16) had the larger G' values in low γ region and exhibited an inflection point at stronger strain, rather than the weak gel (entry 17). Those results indicated that the potential property of the gel was different and the gel obtained from the condition in entry 16 had more hardness and strength against mechanical strain compared to the weak gel (entry 17). In the gel of **2** (entry 16), the observed gel behavior, in which the G' values showed the plateau around $1.0 - 1.2 \times 10$ kPa in low γ region and an inflection point was observed at 1.59 % strain, was consisted with one of the gel of **1** (entry 16). G' and G'' vs γ plots of **1** and **2** are shown in Figure 3 and S2, respectively.

3-4. Vis-NIR spectra; To confirm the coordination structure of **1** as the gel, 15 mM solution in MTH, and powder samples, the visible-near infrared (Vis-NIR) spectra in the range of 500 – 1200 nm were examined. The gel obtained from the solution (20 mM) of **1** in 20% $\text{CH}_2\text{Cl}_2/\text{EtOH}$ was used as a sample for the measurement. The 15 mM solution in MTH showed no gelation behavior. In three samples, a set of shoulder and round maxima at $\lambda_{\text{max}} = \sim 610$ (16.4×10^3) and ~ 995 (10.1×10^3) nm (cm^{-1}), which were characteristic to the octahedron in the Ni(II) complex and were assigned as ${}^3\text{A}_{2\text{g}} \rightarrow {}^3\text{T}_{1\text{g}}$ and ${}^3\text{A}_{2\text{g}} \rightarrow {}^3\text{T}_{2\text{g}}$, respectively, [27] was observed. The octahedral structure by the

coordination of **D1py**₂ to the Ni (II) ion might suggest that the obtained Ni complexes consisted of a chain or a discrete cyclic structures. Vis-NIR spectra in the powder and the gel sample of **1** are shown in Figure 3 and the spectrum for the 15 mM solution of **1** in MTHF is shown in Figure S3.

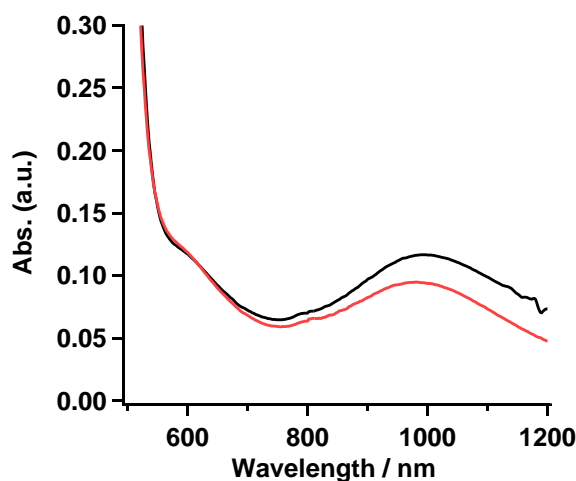


Figure 4. Absorption spectra of **1** in powder (red) and gel sample (black) obtained from the 20 % CH₂Cl₂/EtOH solution.

3-5. Morphology of the gel; To reveal the morphology of **1**, the scanning electron microscopy (SEM) observation of the samples of the xerogel and the powder were performed. The xerogel sample was prepared by freeze-drying the gel of **1**. The SEM images for the xerogel and the powder and exhibited the fibers of 500 - 600 nanometer width and the crystalline solid of micrometer size, respectively. The fibers observed in gel might suggest that **1** had the chain structure formed by alternately binding **D1py**₂ and **Ni(Hex-hfpip)**₂ in molecular level. The morphologies of **1** in the xerogel and the powder are shown in Figure 5. In addition, counts vs width of fiber obtained from SEM image is summarized in Figure S4.

(a)

(b)

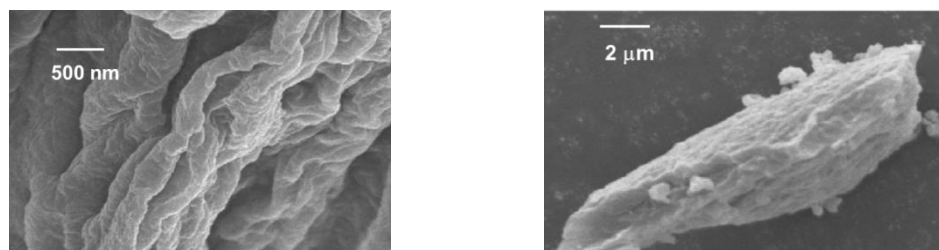


Figure 5. SEM images of xerogel (a) and powder (b) samples for **1**. White lines are scale bars.

3-6. PXRD measurement;

To deduce the molecular structure of the xerogel samples, PXRD measurements of xerogels for **1** and **2** were carried out in the 2θ range of $2 - 10^\circ$ at 23°C . Furthermore the distances obtained from PXRD peaks were compared to one of SXRD result for analogue cobalt chain complex, $[\text{Co}(\text{Br-hfpip})_2\text{D1py}_2]_n$, reported previously (Figure S1').^[21] In the crystal structure of $[\text{Co}(\text{Br-hfpip})_2\text{D1py}_2]_n$, two pyridine rings in **D1py**₂ coordinated to Co ion in *trans* configuration and the distances of one pitch, one unit, and the width of the chain complex, which corresponded to A, B and C in Figure S1', were 22.0, 10.0, and 13.7 Å, respectively.

The xerogel samples obtained from freeze-drying gel of **1** (entry 16) and **2** after removed powder (entry 16) were used. As results of PXRD measurements, same patterns between **1** and **2**, in which two intense peaks in small angle regions and some broadening peaks in small and wide angle regions, were clearly observed. The two intense peaks at 3.81 and 5.74° for **1** and 3.70 and 5.63° for **2** corresponded to the distances of 22.7 and 15.2 Å for **1** and 23.4 and 15.5 Å for **2**, respectively. When compared the distances obtained from SXRD result of analogue $[\text{Co}(\text{Br-hfpip})_2\text{D1py}_2]_n$, the distances due to former and latter peaks in two intense peaks were consisted with those of one pitch within the chain and the width of chain, respectively (A and C in Figure S1'). Furthermore, the weak broadening peaks at 9.0 (9.6) and 8.8° (9.8 Å) for **1** and **2** in PXRD were observed at similar distances to one complex unit (B in Figure S1') in a chain. Accordingly, the resulting PXRD patterns

indicated that the each xerogel of **1** and **2** formed the similar chain structure, in which coordination geometry of the pyridine rings in **D1py**₂ might be *trans* configuration such as analogue [Co(Br-hfpip)₂D1py₂]_n.

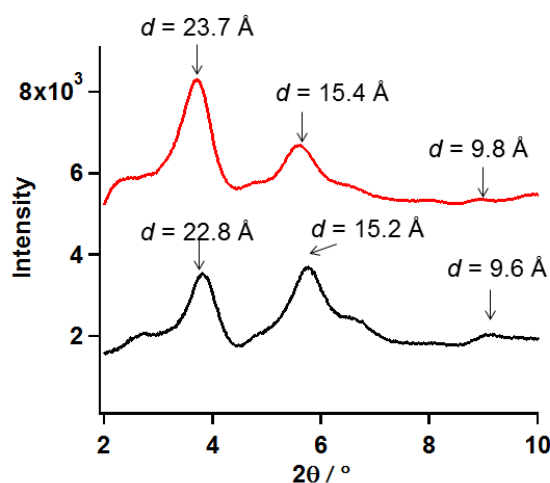


Figure 6. PXRD patterns of the xerogel samples of **1** (black) and **2** (red) in the 2θ range of 2 – 10° at 23 °C.

3-7. Magnetic properties; To understand the magnetic interaction of between nickel(II) ion and the organic spin quantitatively, the magnetic measurements for the reference complex **3** together with **1** were performed by SQUID magneto/susceptometer.

3-7-1. Complex 3: The microcrystalline form of **3** was used as the sample for the magnetic property measurement. The temperature dependence of χ_{mol} values was investigated at a constant field of 5k Oe in the range of 300 – 2 K. The $\chi_{\text{mol}}T$ vs T plot of **3** is shown in Figure 5. The $\chi_{\text{mol}}T$ value at 300 K was $2.2 \text{ cm}^3\text{Kmol}^{-1}$, which was slightly larger than the theoretical value ($2.0 \text{ cm}^3\text{Kmol}^{-1}$) calculated from summation of $\chi_{\text{mol}}T$ value, in which magnetically isolated two **4NOpys** with $S = 1/2$ ($g = 2$) and one Ni(II) ion with $S = 2/2$ ($g = 2.2$).^[28] On cooling, the $\chi_{\text{mol}}T$ values gradually increased and reached to the round maximum ($2.8 \text{ cm}^3\text{Kmol}^{-1}$) at 35 K, indicating that a

ferromagnetic interaction took place. The maximum value was close to the theoretical value ($3.0 \text{ cm}^3\text{Kmol}^{-1}$) of the paramagnetic species carrying $S = 4/2$ when $g = 2$. On cooling below 35 K, the $\chi_{\text{mol}}T$ values abruptly decreased to $0.9 \text{ cm}^3\text{Kmol}^{-1}$ at 2.0 K, indicating that the intermolecular antiferromagnetic interaction operated. In the SXRDR result of **3**, the short contacts of 3.18 \AA between the NO in aminoxy and the C(β) carbon in pyridine rings were observed. These short contacts might cause the intermolecular antiferromagnetic interaction below 35 K.

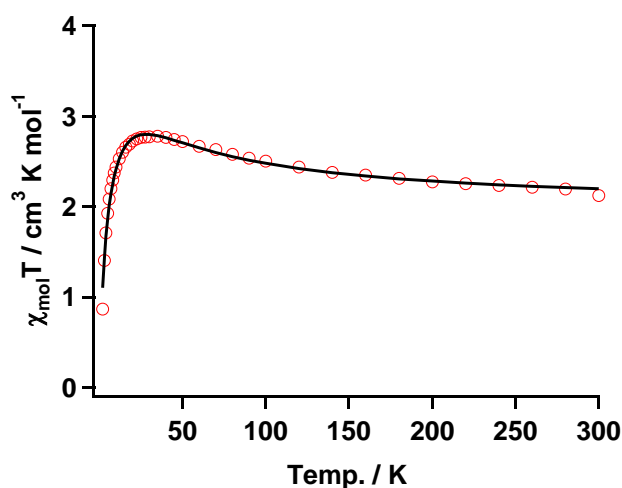


Figure 7. $\chi_{\text{mol}}T$ vs T plot of **3** with the fitting result (solid black line) according to the three spin model in eq. (1). The parameters are shown in the text.

The thermal profile of χ_{mol} values was applied to fitting of a linear three spin model: $H = -J(S_{\text{Ni}}S_1 + S_{\text{Ni}}S_2)$, and the theoretical equation (1), where J/k_{B} , N , k_{B} , μ_{B} , θ denote the magnetic coupling parameter, Avogadro number, Boltzman constant, Bohr magneton, and Weiss constant, respectively, fitted the experimental data. The values obtained by fitting were $g = 2.14$, $J/k_{\text{B}} = 26.7 \text{ K}$, and $\theta = -4.21 \text{ K}$, respectively, indicating that ferromagnetic interaction between Ni(II) and aminoxy through the pyridine rings took place and **3** was species with $S = 4/2$ in the ground state. In contrast, the obtained negative θ value indicated that intermolecular interaction of **3** antiferromagnetically took

place. The fitting result is shown in Figure 7 as the solid line.

$$\chi_{\text{mol}}T = \frac{N g^2 \mu_{\text{B}}^2 T}{2 k_{\text{B}} (T - \theta)} \frac{20 + 4 \exp(-2 J/k_{\text{B}}/T) + 4 \exp(-4 J/k_{\text{B}}/T)}{5 + 3 \exp(-2 J/k_{\text{B}}/T) + 3 \exp(-4 J/k_{\text{B}}/T) + \exp(-9 J/k_{\text{B}}/T)}$$

where $N = 6.022 \times 10^{23}$, $k_{\text{B}} = 1.38 \times 10^{-16}$, $\mu_{\text{B}} = 9.27 \times 10^{-21}$ eq. (1)

The thermal profile in the $\chi_{\text{mol}}T$ vs T plot for the discrete complex of **3** indicated that aminoxy ferromagnetically interacted with Ni(II) ion of **Ni(Hex-hfpip)₂** through the pyridine rings. This result indicated that the magnetic coupling of the carbene generated by photolysis of **1** with the Ni (II) ion might be ferromagnetic.

3-7-2. Complex 1; To understand the magnetic property of **1**, the thermal profiles of χ_{mol} values for the samples of gel, frozen solution, and powder before and after irradiation were investigated. The gel (20 mM, 50 μl) of **1** obtained from the 20% $\text{CH}_2\text{Cl}_2/\text{EtOH}$ solution and the solution (15 mM, 50 μl) of **1** in MTHF was used as the sample. The precipitates obtained from a mixed solution of **D1py₂** and **Ni(Hex-hfpip)₂** in CH_2Cl_2 were used as a powder sample. These samples were photolyzed in the sample room inside the SQUID magneto/susceptometer. The irradiation system using the Ar ion laser (514 nm) was reported previously.^[5a] The temperature during photolyses was carefully kept below 10 K. The degree of photolysis of diazo groups and the generation of triplet carbene by irradiation were determined by the M value measurements at 5 K at a constant field of 5 kOe. Upon irradiation, the M values gradually increased. After irradiation over ca. 20 hr, the alteration of M value reached a plateau and the obtained value was much larger than the value before irradiation, indicating that the diazo moieties were photolyzed to generate the triplet carbene. The plots of M vs. irradiation time are shown in Figure S5. After SQUID measurements, the degrees of photolysis were estimated to be 86, 88, and 83 % for the samples of gel, frozen solution, and powder, respectively, from the consumption of the ν_{N_2} absorption in the IR spectra.

The magnetic susceptibility measurements before and after irradiation were performed in the temperature range of 50 - 2 K under conditions similar to that for **3**. The $\chi_{\text{mol}}T$ vs T plots for the samples of 20 mM gel, 15 mM frozen solution, and powder of **1** before and after irradiation are summarized in Figure 8.

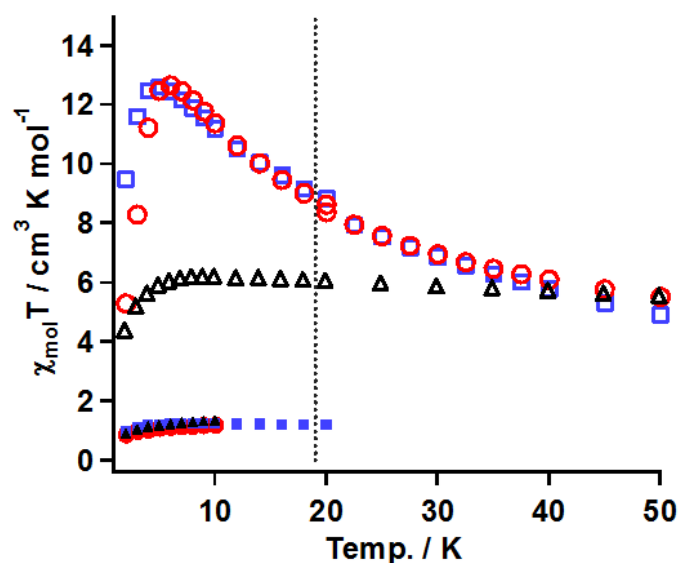


Figure 8. $\chi_{\text{mol}}T$ vs T plots before (filled marks) and after (blank marks) irradiation of **1** for samples of 20 mM gel (red circles), powder (blue squares), and 15 mM frozen solution (black triangles). Thermal profiles of the gel and powder samples were carried out under 5 kOe (50 – 20 K) and 0.5 kOe (below 18 K), respectively. A dotted delimiter line was put on 19 K.

(A) Gel sample. The $\chi_{\text{mol}}T$ value before irradiation was $1.1 \text{ cm}^3\text{Kmol}^{-1}$ at 20 K, which was consistent with the value magnetically isolated Ni(II) spin when $g = 2.0$. On cooling, the $\chi_{\text{mol}}T$ value was constant until 2 K, suggesting that the ground state was $S = 2/2$. After irradiation for 33 hr, the χ_{mol} values were collected at the constant field of 5 kOe in the temperature range of 50 - 20 K and at 0.5 kOe in 18 – 2 K. The $\chi_{\text{mol}}T$ value at 50 K was $5.5 \text{ cm}^3\text{Kmol}^{-1}$. This value was much larger than

magnetically isolated value of $2 \text{ cm}^3 \text{Kmol}^{-1}$, which was calculated from $S = 2/2$ for Ni(II) ion and $S = 2/2$ for triplet carbene, and the value of $3 \text{ cm}^3 \text{Kmol}^{-1}$ calculated by a ferromagnetic Ni(II)-carbene unit with $S = 4/2$. The $\chi_{\text{mol}}T$ value at 50 K indicated that the ferromagnetic interaction between the the triplet carbene and the Ni(II) ion took place to form a species with high-spin ground state. On cooling, the $\chi_{\text{mol}}T$ value gradually increased and reached a maximum of $12.7 \text{ cm}^3 \text{Kmol}^{-1}$ at 6 K. The observed increase of the $\chi_{\text{mol}}T$ values indicated that the correlation length of the magnetic chain became longer with decreasing temperature. The magnetic correlation length, n , was roughly estimated from eq. (2) and (3).^[29] In the $\ln(\chi_{\text{mol}}T)$ vs T^{-1} plot (Figure S6), the data from 50 – 15 K were fitted by a linear line model, giving the straight line and the value of $\Delta_{\xi} = 13.5 \text{ K}$ from a slope, which was the energy to create a domain wall. In the Heisenberg limit ($|D| \ll |J|$), the value of Δ_{ξ} was correlated to $4S_{\text{T}}^2 \sqrt{|JD|}$ and $k_{\text{B}}T \ln(2n)$ represented in eq. (2). Those parameters of J , D , S_{T} , k_{B} , T^* and n denote the magnitude of magnetic interaction and zero-field splitting value within Ni-triplet carbene complex, spin quantum number of one unit ($S = 4/2$ in this case), Boltzmann constant, the maxima value of $\chi_{\text{mol}}T$ and the correlation length, respectively. When using the value of 13.5 K of Δ_{ξ} and 6 K of T^* in eq. (2) obtained from the $\chi_{\text{mol}}T$ vs T plot (Figure 8), the value of $n = 5$ was led.

$$\Delta_{\xi} = k_{\text{B}}T^* \ln(2n) = 4S_{\text{T}}^2 \sqrt{|JD|} \quad \text{eq. (2)}$$

$$\chi_{\text{n}}T/C_{\text{eff}} \approx n \quad \text{eq. (3)}$$

In eq.(3), an effective Curie constant, C_{eff} , in **1** after irradiation was roughly deduced to the value of $3 \text{ cm}^3 \text{Kmol}^{-1}$ calculated by a ferromagnetic Ni(II)-carbene unit with $S = 4/2$. From the maximum value of $12.7 \text{ cm}^3 \text{Kmol}^{-1}$ at 6 K in $\chi_{\text{mol}}T$ vs T plot, the n value, correlation length, was estimated to be 4 units. From the results of eq. (2) and (3), accordingly, n value was estimated to be 4 - 5 units. Below 5 K, the $\chi_{\text{mol}}T$ values steeply decreased due to intermolecular antiferromagnetic interaction.

(B) In the frozen solution sample. Before irradiation, the thermal profile of $\chi_{\text{mol}}T$ values was

similar to that for the gel sample. After irradiation for 19 hr, the χ_{mol} values were collected under conditions similar to that for the gel sample. The $\chi_{\text{mol}}T$ value at 50 K was $5.5 \text{ cm}^3\text{Kmol}^{-1}$, which was similar to the gel sample. On cooling, interestingly, the $\chi_{\text{mol}}T$ values were nearly constant until 6 K and then decreased below 6 K. The constant $\chi_{\text{mol}}T$ values in the range 50 – 6 K and their values of $5.5 - 6 \text{ cm}^3\text{Kmol}^{-1}$ might suggested that ferromagnetic species with a high-spin ground state formed and their S values were $S = 6/2$, respectively.

(C) Powder The thermal profiles before and after irradiation for 20 hr were similar to those of the gel sample. The maximum value after irradiation of $\chi_{\text{mol}}T$ was $12.6 \text{ cm}^3\text{Kmol}^{-1}$ at 5 K corresponding to the correlation length of 4 – 5 units, which was comparable with the value of the gel sample.

3-8. Molecular and magnetic structures of 1 in gel, solution, and powder samples. Vis-NIR spectra of the gel, the solution, and the powder samples of **1** showed a set of shoulder and round absorption maxima at $\lambda_{\text{max}} = \sim 610 (16.4 \times 10^3)$ and $\sim 995 (10.1 \times 10^3) \text{ nm (cm}^{-1})$ due to the octahedral Ni(II) complex, suggesting that the pyridine rings in **D1py**₂ coordinated to the Ni(II) ions to form a chain and a cyclic structure. In magnetic measurements after irradiation of gel and frozen solution samples, the $\chi_{\text{mol}}T$ values at 50 K for both samples were similar at $5.5 \text{ cm}^3\text{Kmol}^{-1}$. This value of $5.5 \text{ cm}^3\text{Kmol}^{-1}$ was larger than $3.0 \text{ cm}^3\text{Kmol}^{-1}$ for the ferromagnetic one unit (carbene-Ni(II) ion) with $S = 4/2$, indicating that the generated carbenes ferromagnetically interacted with the Ni(II) ions to form the high-spin species. The reference complex **[Ni(Hex-hfpip)₂(4NOpy)₂]** also showed ferromagnetic interaction with $J/k_{\text{B}} = 26.7 \text{ K}$ between the aminoxyl and the Ni(II) through the pyridine ring. The thermal profiles of the $\chi_{\text{mol}}T$ values in the temperature range of 50 – 7 K showed different magnetic behaviors. In the $\chi_{\text{mol}}T$ vs. T plots, the $\chi_{\text{mol}}T$ values for the gel sample gradually increased with decreasing temperature, while those for the frozen solution sample were nearly

constant. The observed increase of the $\chi_{\text{mol}}T$ values for gel sample indicated that the correlation length of the magnetic chain became longer with decreasing the temperature. In contrast, the observed temperature-independent thermal profile of the $\chi_{\text{mol}}T$ values for the frozen solution sample might suggest the formation of discrete high-spin species having a cyclic structure. The powder sample showing the similar magnetic behavior to that for the gel might have a chain structure. The magnetic behaviors observed in the gel and powder samples were similar to that for the copper chain complex, $[\text{Cu}(\text{hfac})_2(\text{D1py}_2)]_n$ reported previously.^[9b] Plausible molecular and magnetic structures of **1** in the gel and the frozen solution are depicted in Figure 9.

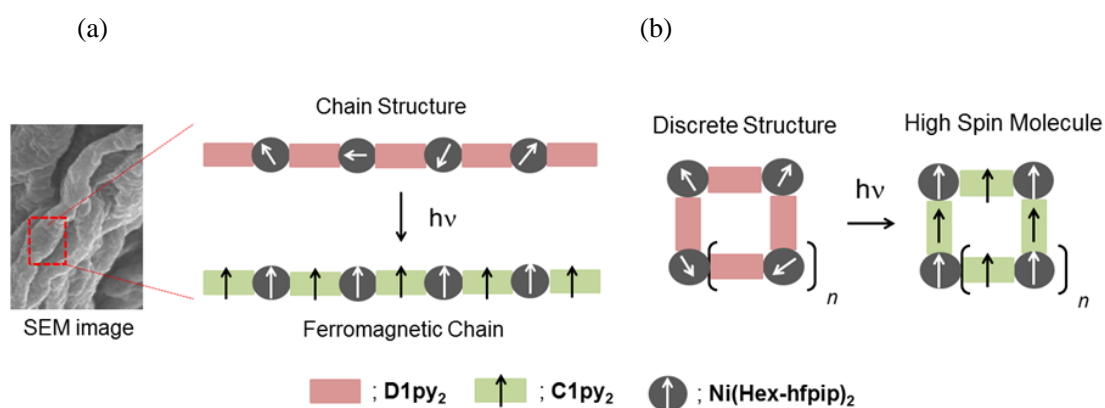


Figure 9. Plausible molecular and magnetic structures in the gel (a) and the frozen solution (b) of **1**.

4. Conclusion

The octahedral Ni(II) complexes consisting of **D1py**₂ and **Ni(R-hfpip)**₂; R = *n*-hexyl (**1**) and *n*-octyl (**2**), were prepared. In the gelation test and the rheological measurements, **1** and **2** was found to become a gel in 20 mM solution of 20 %CH₂Cl₂/EtOH at -4 °C. In SEM image of the xerogel obtained from freeze- drying the gel sample, fibers with the width of ca. 500 – 600 nm were observed. The resulting gel exhibited magnetic behavior of the ferromagnetic chain after irradiation. No example of a gel showing such strong magnetic interaction has been reported. Attempts to

construct the magnetic gel showing the magnetic behavior of single-chain magnets (SCMs) by using anisotropic transition metal ions are in progress.

Acknowledgements

This work was partially supported by Platform for Drug Discovery, Informatics, and Structural Life Science from the Ministry of Education, Culture, Sports, Science and Technology (MEXT), Japan. S. K. appreciates Grants-in-Aid for Scientific Research (B)(2)(No. 25288038) from the Japan Society for the Promotion of Science (JSPS), and PRESTO program on Molecular Technology from Japan Science Technology Agency (JST).

Electronic supplementary information (ESI) available:

Additional X-ray structure of **3**. Rheological measurement of the gel for **2**. Vis-NIR spectrum in 15 mM MTHF solution sample of **1**. M vs *Irradiation time* plots. $\ln(\chi_{\text{mol}}T)$ vs T plot after irradiation of the gel for **1**. CCDC 1406724 for **3**. For ESI and crystallographic data in CIF or other electronic format see DOI: 10.1039/xxxxxxx.

References and Note

- (a) D. Gatteschi, R. Sessoli, J. Villain, *Molecular Nanomagnets*, Oxford University Press, New York, **2006**. (b) G. Christou, D. Gatteschi, D.N. Hendrickson, R. Sessoli *MRS Bull.* **2000**, *25*, 66.
- (a) Z.-X., Wang, X. Zhang, Y.-Z., Zhang, M.-X., Li, H. Zhao, M. Andruh, K. R. Dunbar *Angew.*

- Chem. Int. Ed.* **2014**, *53*, 11567. (b) R. Clérac, H. Miyasaka, M. Yamashita, C. Coulon *J. Am. Chem. Soc.* **2002**, *124*, 12837. (c) A. Caneschi, D. Gatteschi, N. Lalioti, C. Sangregorio, R. Sessoli, G. Venturi, A. Vindigni, A. Rettori, M. G. Pini, M. A. Novak *Angew. Chem. Int. Ed.* **2001**, *40*, 1760.
- 3.(a) K. R. Meihaus, J. R. Long *J. Am. Chem. Soc.* **2013**, *135*, 17952. (b) D.N. Woodruff, R.E.P. Winpenny, R.A. Layfield *Chem. Rev.* **2013**, *113*, 5110.
4. (a) M. Jenkins, T. Hümmer, M. J. Martínez-Pérez, J. García-Ripoll, D. Zueco, F. Luis *New J. Phys.* **2013**, *15*, 095007. (b) G. Kresse, J. Hafner *Phys. Rev. B.* **1994**, *49*, 14251.
5. (a) N. Koga, S. Karasawa *Bull. Chem. Soc. Jpn.* **2005**, *78*, 1384. (b) I.-R. Jeon, J.G. Park, D. J. Xiao, T.D. Harris *J. Am. Chem. Soc.* **2013**, *135*, 16845. (c) J. D. Rinehart, M. Fang, W.J. Evans, J.R. Long *Nat. Chem.* **2011**, *3*, 538.
6. O. Kahn, *Molecular Magnetism*, Wiley-VCH Publishers, Weinheim, **1993**.
7. (a) S. Kanegawa, S. Karasawa, M. Nakano, N. Koga *Chem. Commun.* **2004**, 3590. (b) M. Kitano, Y. Ishimaru, K. Inoue, N. Koga, H. Iwamura *Inorg. Chem.* **1994**, *33*, 6012.
8. (a) S. Karasawa, N. Koga *Inorg. Chem.* **2011**, *50*, 5186. (b) S. Karasawa, D. Yoshihara, N. Watanabe, M. Nakano, N. Koga *Dalton Trans.* **2008**, 1418. (c) S. Karasawa, G. Zhou, H. Morikawa, N. Koga *J. Am. Chem. Soc.* **2003**, *125*, 13676.
9. (a) S. Karasawa, Y. Sano, T. Akita, N. Koga, T. Itoh, H. Iwamura, P. Rabu, M. Drillon *J. Am. Chem. Soc.* **1998**, *120*, 10080. (b) Y. Sano, M. Tanaka, N. Koga, K. Matsuda, H. Iwamura, P. Rabu, M. Drillon *J. Am. Chem. Soc.* **1997**, *119*, 8246.
10. (a) D. Yoshihara, S. Karasawa, N. Koga *Inorg. Chim. Acta* **2015**, *428*, 57. (b) D. Yoshihara, S. Karasawa, N. Koga *Polyhedron* **2011**, *30*, 3211. (c) D. Yoshihara, S. Karasawa, N. Koga *J. Am. Chem. Soc.* **2008**, *130*, 10460.
11. (a) S. Karasawa, K. Nakano, D. Yoshihara, N. Yamamoto, J. Tanokashira, T. Yoshizaki, Y.

- Inagaki, N. Koga *Inorg. Chem.* **2014**, *53*, 5447. (b) S. Karasawa, K. Nakano, J. Tanokashira, N. Yamamoto, T. Yoshizaki, N. Koga *Dalton Trans.* **2012**, 13656. (c) S. Karasawa, D. Yoshihara, N. Watanabe, M. Nakano, N. Koga *Dalton Trans.* **2008**, 1418. (d) H. Tobinaga, M. Suehiro, T. Itoh, G. Zhou, S. Karasawa, N. Koga *Polyhedron*, **2007**, *26*, 1905.
12. (a) N. Annabi, K. Tsang, S. M. Mithieux, M. Nikkhah, A. Ameri, A. Khademhosseini, A. S. Weiss *Adv. Funct. Mater.* **2013**, *23*, 4950. (b) H. C. Fiegel, C. Lange, U. Kneser, W. Lambrecht, A. R. Zander, X. Rogiers, D. Kluth *J. Cell. Mol. Med.* **2006**, *10*, 577.
13. (a) J. B. Goodenough, Y. Kim *Chem. Mater.* **2010**, *22*, 587. (b) P. Wang, S. M. Zakeeruddin, J. E. Moser, M. K. Nazeeruddin, T. Sekiguchi, M. Grätzel *Nature Mater.* **2003**, *2*, 402.
14. Y.-H. Kim, J.-S. Heo, T.-H. Kim, S. Park, M.-H. Yoon, J. Kim, M. S. Oh, G.-R. Yi, Y.-Y. Noh, S. K. Park *Nature*, **2012**, *489*, 128.
15. T. Ono, T. Sugimoto, S. Shinkai, K. Sada *Nature Mater.* **2007**, *6*, 429.
16. (a) Y. Wu, Y. Hirai, Y. Tsunobuchi, H. Tokoro, H. Eimura, M. Yoshio, S. Ohkoshi, T. Kato *Chem. Sci.*, **2012**, *3*, 3007. (b) M. Shirakawa, N. Fujita, H. Shimakoshi, Y. Hisaeda, S. Shinkai *Tetrahedron*, **2006**, *62*, 2016.
17. (a) G. Nandi, H. M. Titi, R. Thakuria, I. Goldberg *Cryst. Growth Des.* **2014**, *14*, 2714. (b) J. Park, J. H. Lee, J. Jaworski, S. Shinkai, J. H. Jung *Inorg. Chem.* **2014**, *53*, 7181. (c) C. Gonçalves, Y. Lalatonne, L. Melro, G. Badino, M. F. Ferreira, L. David, C. F. G. C. Geraldés, L. Motte, J. A. Martins, F. M. Gama *J. Mater. Chem. B*, **2013**, *1*, 5853. (d) M. Takauchi, S. Tanaka, S. Shinkai *Chem. Comm.* **2005**, 5539.
18. H. Hayashi, K. Ohkubo, S. Karasawa, N. Koga *Langmuir*, **2011**, *27*, 12709.
19. (a) H. Kamata, Y. Akagi, Y. Kayasuga-Karita, U.-i. Chung, T. Sakai *Science*, **2014**, *343*, 873. (b) K. Takemura, H. Ajiro, T. Fujiwara, M. Akashi *RSC Advances*, **2014**, *4*, 63.
20. (a) H. Komatsu, S. Matsumoto, S. Tamaru, K. Kaneko, M. Ikeda, I. Hamachi *J. Am. Chem. Soc.*

- 2009**, *131*, 5580. (b) L. A. Estroff, A. D. Hamilton *Chem. Rev.* **2004**, *104*, 1201. (c) S. Kiyonaka, K. Sada, I. Yoshimura, S. Shinkai, N. Kato, I. Hamachi *Nature Mater.* **2004**, *3*, 58. (d) J. H. Jung, S. Shinkai, T. Shimizu *Chem.—Eur. J.* **2002**, *8*, 2684.
21. S. Karasawa, N. Koga *Inorg. Chem.* **2011**, *50*, 2055.
22. *SHELX 97*: G. M. Sheldrick *Acta Crystallogr.* **2008**, *A64*, 112.
23. *Crystal Structure 3.5.1*: Crystal Structure Analysis Package, Rigaku and Rigaku/MSK, 2000–2003, 9009 New Trails Dr. The Woodlands, TX 77381, USA.
24. X.-D. Xu, J. Zhang, L.-J. Chen, X.-L. Zhao, D.-X. Wang, H.-B. Yang *Chem. – E. J.* **2012**, *18*, 1659.
25. K. Matsumoto, A. Shundo, M. Ohno, S. Fujita, K. Saruhashi, N. Miyachi, K. Miyaji, K. Tanaka *Phys. Chem. Chem. Phys.* **2015**, *17*, 2192.
26. (a) S. Bhattacharya, S. Sengupta, S. Bala, A. Goswami, S. Ganguly, R. Mondal, *Cryst. Growth Des.* **2014**, *14*, 2366. (b) J. H. Lee, S. Kang, J. Y. Lee, J. Jaworski, J. H. Jung *Chem. – Eur. J.* **2013**, *19*, 16665.
27. (a) M. Arakawa, N. Suzuki, S. Kishi, M. Hasegawa, K. Satoh, E. Horn, Y. Fukuda *Bull. Chem. Soc. Jpn.* **2008**, *81*, 127. (b) K. Miyamoto, M. Sakamoto, C. Tanaka, E. Horn, Y. Fukuda *Bull. Chem. Soc. Jpn.* **2005**, *78*, 1061.
28. (a) P. B. Sczaniecki, J. Lesniak, *J. Magn. Reson.* **1982**, *46*, 185. (b) J. Reedijk, B. Nieuwenhuijse, *Rec. Trav. Chim.* **1972**, *91*, 533.
29. (a) H. Miyasaka, M. Julve, M. Yamashita, R. Clérac *Inorg. Chem.* **2009**, *48*, 3420. (b) M. Ferbinteanu, H. Miyasaka, W. Wernsdorfer, K. Nakata, K. Sugiura, M. Yamashita, C. Coulon, R. Clérac *J. Am. Chem. Soc.* **2005**, *127*, 3090. (c) C. Coulon, R. Clérac, R. Leccrem, W. Wernsdorfer, H. Miyasaka *Phys. Rev. B* **2004**, *69*, 132408.